Power Balance of Cascaded H-Bridge Multilevel Converters for Large-Scale Photovoltaic Integration

Yifan Yu, *Student Member, IEEE*, Georgios Konstantinou, *Member, IEEE*, Branislav Hredzak, *Senior Member, IEEE*, and Vassilios G. Agelidis, *Senior Member, IEEE*

***Abstract*—Multilevel cascaded H-bridge converters are promising candidates for large-scale photovoltaic power plants. They allow direct connection to medium-voltage distribution networks without the presence of bulky line frequency power transformers. Owing to the stochastically variable nature of irradiance level, ambient temperature, and other factors, power levels in the three phases are expected to be unequal. The power imbalance condition creates unexpected problems with this topology, which was initially designed to operate under balanced power conditions. To deal with this issue, the paper proposes three novel zero-sequence injection methods as an expansion to the conventional zero-sequence injection method. Results obtained from simulations and a 430-V 8-kW three-phase seven-level cascaded H-bridge prototype are presented to verify the effectiveness and feasibility of the proposed methods.**

***Index Terms*—AC–DC power converters, cascaded H-bridge (CHB) converter, multilevel converter, photovoltaics (PV).**

NOMENCLATURE

$\mathbf{V_{ga}}, \mathbf{V_{gb}}, \mathbf{V_{gc}}$	Three-phase grid voltage vectors.
V_g	Grid voltage (line-to-line) (rms).
V_{gd}	Grid voltage (direct-axis component) (rms).
$\mathbf{V_a}, \mathbf{V_b}, \mathbf{V_c}$	Three-phase converter output voltage vectors.
v_a, v_b, v_c	Three-phase converter output voltages (instantaneous values).
v_a^+, v_b^+, v_c^+	Positive-sequence component of three-phase converter output voltages (instantaneous values).
V^+	Positive-sequence component of three-phase converter output voltages (rms).
v_a^1, v_b^1, v_c^1	Fundamental frequency component of three-phase converter output voltages (instantaneous value).
V_a^1, V_b^1, V_c^1	Fundamental frequency component of three-phase converter output voltages (rms).
$\beta_a, \beta_b, \beta_c$	Phase angles of fundamental frequency component of three-phase converter output voltages.
v^3	Third harmonic component of three-phase converter output voltages (instantaneous value).
$\mathbf{I_{ga}}, \mathbf{I_{gb}}, \mathbf{I_{gc}}$	Three-phase grid current vectors.
i_{ga}, i_{gb}, i_{gc}	Three-phase grid currents (instantaneous values).
I_g	Grid current (rms).
$\mathbf{V^0}$	Fundamental frequency zero-sequence vector.
v^0	Fundamental frequency zero-sequence component (instantaneous value).
V^0	Fundamental frequency zero-sequence component (rms).
v^{0*}, v^{0**}	Fictitious fundamental frequency zero-sequence component (instantaneous value).
θ	Phase angle of fundamental frequency zero-sequence component.
$P_{\rm nom}$	Three-phase nominal power (peak).
$\lambda_a, \lambda_b, \lambda_c$	Three-phase power generation ratios.
ω	Angular frequency.
α	Phase angle between converter output voltage vectors and grid current vectors.
$v_{\rm dc}$	Capacitor (dc side) voltage of H-bridges.

Manuscript received October 9, 2014; revised December 14, 2014; accepted February 13, 2015. Date of publication February 24, 2015; date of current version September 21, 2015. Recommended for publication by Associate Editor B. Choi.

The authors are with the Australian Energy Research Institute and the School of Electrical Engineering and Telecommunications, University of New South Wales, Sydney, N.S.W. 2052, Australia (e-mail: yifan.yu@student.unsw.edu.au; g.konstantinou@unsw.edu.au; b.hredzak@unsw.edu.au; vassilios.agelidis@unsw.edu.au).

Color versions of one or more of the figures in this paper are available online at http://ieeexplore.ieee.org.

Digital Object Identifier 10.1109/TPEL.2015.2406315

I. INTRODUCTION

LARGE-SCALE centralized photovoltaic (PV) power plants are considered more attractive than small-scale residential installations, since they provide lower costs per watt and are operationally closer to conventional power plants [1]–[5]. Most of the commercially available converters for PV power plants are traditional two-level voltage-source converters with rated power lower than 1.5 MW [6], [7]. Multilevel high-power PV converters, operating with reduced switching frequency and losses and, hence, increased efficiency, are being explored by researchers worldwide as a promising alternative [8]–[23]. The multilevel cascaded H-bridge (CHB) converter is considered one of the most suitable candidates for next-generation PV plant converters [12]–[21], owing to the presence of multiple separate low-voltage dc links, which are readily available in PV systems.

A three-phase seven-level CHB converter (see Fig. 1) consists of nine H-bridges (three per phase), each fed by multiple strings of PV modules via separate dc–dc converters. The regulation of the dc-side capacitor voltages $v_{\rm dc}$ is performed via a voltage controller, while each dc–dc converter conducts independent maximum power point tracking (MPPT) to maximize the captured power. A high-frequency isolation transformer is

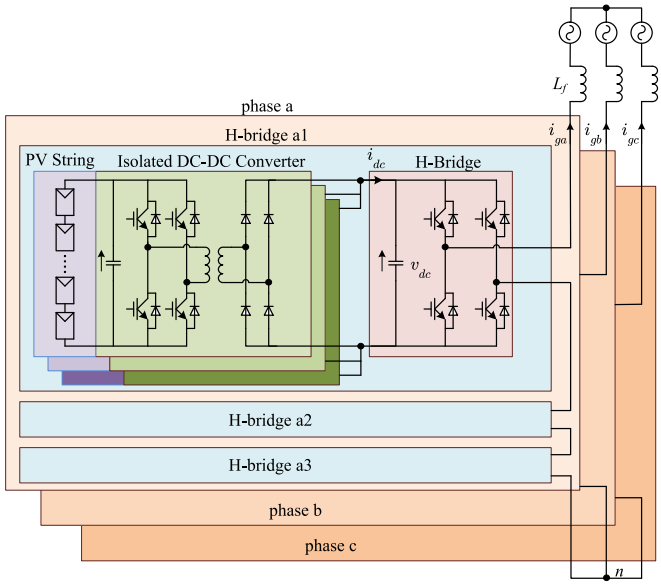

Fig. 1. Three-phase seven-level CHB converter.

included in the dc–dc converter for two reasons. One is to isolate the PV modules from the grid, because most commercial PV modules are designed to withstand no more than 1000 V between the active part and the grounded frame. The second reason is that the transformer helps to increase the voltage gain of the dc–dc converter so that MPPT can still be achieved under low irradiance levels.

The topology shown in Fig. 1 features several merits. The required switching frequency and resulting power losses are less than the conventional two-level solution, since the converter output voltages exhibit multilevel waveforms. It can also be extended to more levels without much effort owing to its modular structure. Additionally, bulky and heavy line-frequency power transformers can be eliminated, because galvanic isolation has been implemented via compact high-frequency transformers embedded in the dc–dc stage, and by cascading more H-bridges the converter is able to reach medium voltage levels. A recent evaluation of the CHB for large-scale PV applications demonstrates that multilevel CHB converters can reduce the levelized cost of energy, compared with state-of-the-art two-level converters [12].

A vital problem stemming from the independent operation of multiple dc links is that the power generated by the PV modules connected to each bridge can be unequal. This power imbalance can be caused by nonuniform solar irradiance, unequal ambient temperatures, or inconsistent module degradation. However, most grid codes mandate three-phase balanced currents [24]. Modified control methods are thus needed to deliver balanced three-phase currents to the grid; otherwise, the converter may have to be disconnected from the grid, resulting in wasted power.

The essence of the power imbalance problem lies in the delivery of three-phase balanced currents to the grid, with unbalanced PV power generation in each bridge. The problem can be further classified into two categories: 1) the interphase (clustered) power imbalance, which occurs when each phase generates a different amount of power; and 2) the interbridge (individual) power imbalance, which happens when each bridge in the same phase leg generates a different amount of power.

A continuous time-domain power balancing control algorithm has been presented to solve the interbridge imbalance of a single-phase CHB converter [15]. A corresponding discrete method has also been proposed to deal with the same problem [16]. However, in both papers, owing to the absence of interfacing dc–dc converters, the capacitor voltages of H-bridges have to be varied to achieve local MPPT, resulting in a suboptimal harmonic spectrum. Moreover, the lack of galvanic isolation limits the operational dc voltage owing to safety requirements; thus, making it less attractive for high-power applications.

The injection of a zero-sequence component into the converter output voltages has been proven effective in solving the interphase power imbalance of three-phase CHB converters [17]–[20]. A weighted min–max (WMM) zero-sequence injection method was proposed in [19] and [20], which modifies the converter output voltages with the ratio of actual power generation. Although WMM is simple to implement, it is not able to provide sufficiently accurate results for the power balance control. A fundamental frequency zero-sequence injection (FFZSI) that redistributes the generated power among the three phases has been derived through the instantaneous power theory [17] and phasor diagrams [18], respectively. Although this zero-sequence injection method features clear physical explanation and simple implementation, it is certainly not the best option. The injection of the zero sequence comes at the expense of increasing converter output voltages. While the converter output voltages increase with the severity of the power imbalance and reach the limit set by the dc-side voltages, the target of delivering balanced grid currents with the zero-sequence injection fails. FFZSI exploits the relatively low dc-side voltages in such an inefficient way that the voltage limit is easily reached with a slight power imbalance. The interphase and interbridge power imbalance can solved with different and independent approaches.

The objective of this paper is to propose and experimentally verify three novel zero-sequence injection methods to deal with the interphase power imbalance problem of CHB converters in large-scale PV power plants. Compared with the conventional solution (FFZSI), the proposed methods offer better utilization of the dc-side voltages by modifying the harmonic components of the injected zero sequence. The new methods are able to generate three-phase balanced grid currents under relatively severe power imbalance conditions, where the conventional solution fails.

The rest of the paper is organized as follows. Section II reviews the existing method (FFZSI) and the corresponding mechanism of achieving three-phase balanced grid currents with unbalanced PV power generation from the three phases. Three novel methods are subsequently derived in Section III. Section IV describes simulation of a 10-MW PV power plant, before experimental results from a scaled-down laboratory prototype are provided in Section V to validate the effectiveness and feasibility of the presented methods. Final conclusions are drawn in Section VI.

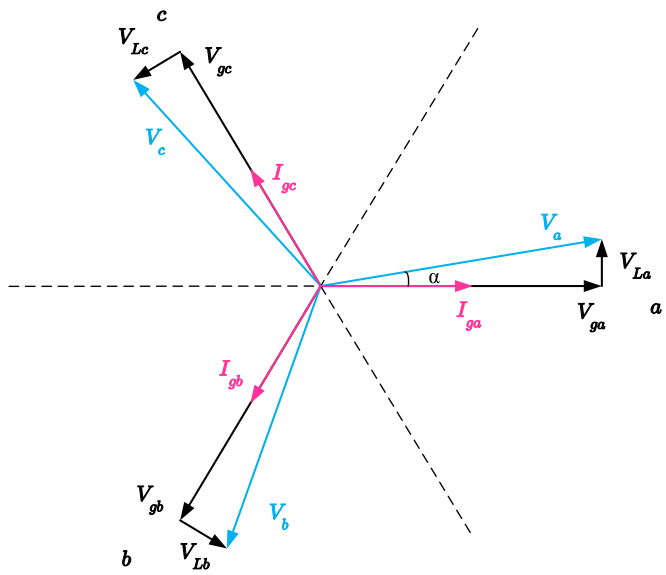

Fig. 2. Phasor diagram for balanced operation of a CHB converter.

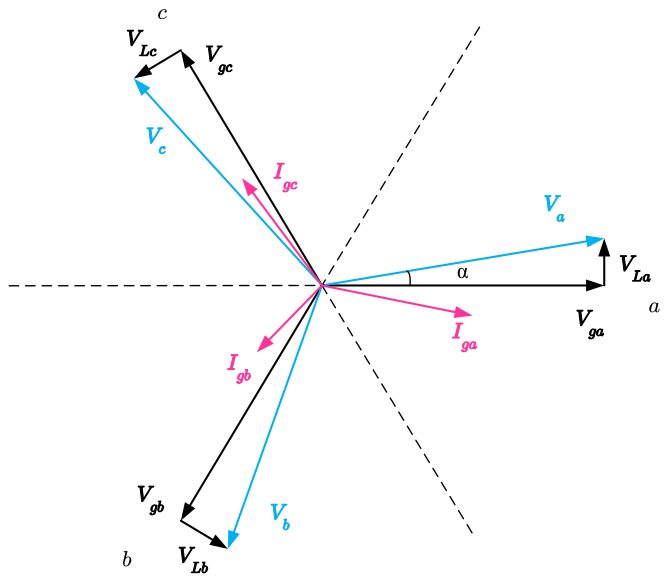

Fig. 3. Phasor diagram for unbalanced operation of a CHB converter.

II. Review of the Existing Method

For CHB converters with equal amounts of power generated in each phase, the three-phase converter output voltages are expected to be symmetrical with equal amplitude and 120° phase displacement from one another; therefore, are the grid current vectors. In Fig. 2, $\mathbf{V_{ga}}$, $\mathbf{V_{gb}}$, and $\mathbf{V_{gc}}$ and $\mathbf{I_{ga}}$, $\mathbf{I_{gb}}$, and $\mathbf{I_{gc}}$ represent the grid voltage and current vectors, respectively, while $\mathbf{V_a}$, $\mathbf{V_b}$, and $\mathbf{V_c}$ represent the converter output voltage vectors. When the power generated by the PV modules connected to different phases is unequal, the three-phase grid currents will be asymmetrical (see Fig. 3) if the converter is still modulated in the same way as when balanced power is generated.

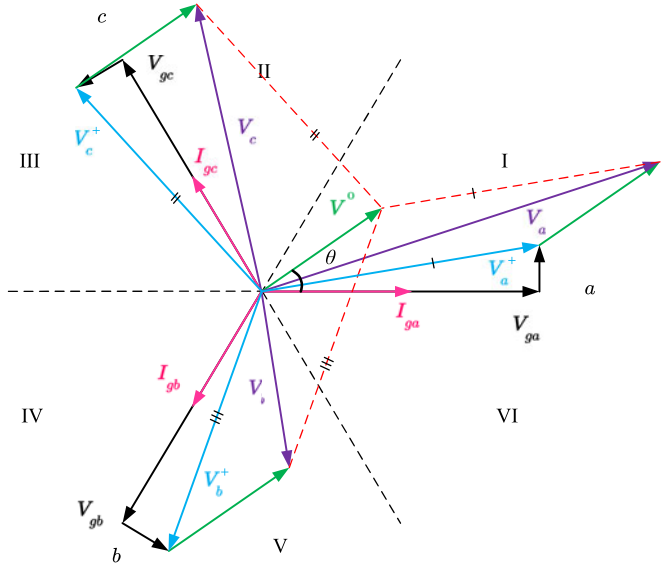

Fig. 4. Phasor diagram for unbalanced operation with FFZSI.

The calculations of power imbalance are based on the power generation ratios λ_a, λ_b, and λ_c, which are defined as the actual generated power of each phase compared to 1/3 of the three-phase nominal power $P_{\rm nom}$ as

$$\lambda_{a,b,c} = \frac{p_{a,b,c}}{P_{\rm nom}/3}. \tag{1}$$

In a generalized unbalanced case, the three-phase power generation ratios are expected to be

$$0 < \lambda_a \neq \lambda_b \neq \lambda_c \leq 1. \tag{2}$$

The injection of a fundamental frequency zero-sequence component into the converter output voltages is able to rebalance the three-phase grid currents [17], [18]. The power generated by the injected zero sequence vector $\mathbf{V^0}$ with the grid current vector of each phase $\mathbf{I_{ga}}$, $\mathbf{I_{gb}}$, and $\mathbf{I_{gc}}$ (see Fig. 4) should be equal to the extra power of that phase after deducting the three-phase average

$$V^0 I_g \cos\theta = \Delta P_a = (\lambda_a - \bar{\lambda})\frac{P_{\rm nom}}{3} \tag{3a}$$

$$V^0 I_g \cos(\theta + 2\pi/3) = \Delta P_b = (\lambda_b - \bar{\lambda})\frac{P_{\rm nom}}{3} \tag{3b}$$

$$V^0 I_g \cos(\theta - 2\pi/3) = \Delta P_c = (\lambda_c - \bar{\lambda})\frac{P_{\rm nom}}{3} \tag{3c}$$

$$\bar{\lambda} = \frac{\lambda_a + \lambda_b + \lambda_c}{3}. \tag{3d}$$

The FFZSI can thus be derived as

$$v^0 = \sqrt{2}V^0 \cos(\omega t + \theta) \tag{4}$$

TABLE I
ZERO-SEQUENCE VECTOR SECTOR

Three-phase Power Generation Ratios	Sector
$\lambda_b < \lambda_c < \lambda_a$	(I)
$\lambda_b < \lambda_a < \lambda_c$	(II)
$\lambda_a < \lambda_b < \lambda_c$	(III)
$\lambda_a < \lambda_c < \lambda_b$	(IV)
$\lambda_c < \lambda_a < \lambda_b$	(V)
$\lambda_c < \lambda_b < \lambda_a$	(VI)

where

$$V^0 = \frac{\sqrt{6}\Delta}{3(\lambda_a+\lambda_b+\lambda_c)}V_g \tag{5a}$$

$$\theta = \begin{cases} \sin^{-1}\left(\frac{\sqrt{6}(\lambda_c-\lambda_b)}{2\Delta}\right) & \text{Sectors (I), (VI)} \\ \frac{2\pi}{3}+\sin^{-1}\left(\frac{\sqrt{6}\,(\lambda_b-\lambda_a)}{2\Delta}\right) & \text{Sectors (II), (III)} \\ \frac{4\pi}{3}+\sin^{-1}\left(\frac{\sqrt{6}\,(\lambda_a-\lambda_c)}{2\Delta}\right) & \text{Sectors (IV), (V)} \end{cases} \tag{5b}$$

$$\Delta = \sqrt{(\lambda_a-\lambda_b)^2+(\lambda_b-\lambda_c)^2+(\lambda_a-\lambda_c)^2} \tag{5c}$$

and the sector can be determined via Table I.

Equation (5) shows that the rms value and phase angle of FFZSI are determined by the grid voltages and the three-phase power generation. The rms value V^0 is expected to increase with the severity of the power imbalance. The maximum converter output voltages are, on the other hand, constrained by the dc-side voltages, just like most voltage-source converters. If the required converter output voltages fall within the limit set by the dc-side voltages, FFZSI is able to deliver balanced grid currents, even with unbalanced power generation. However, when the power imbalance among the three phases increases, the required converter output voltages are likely to exceed the limit, and the method ceases to function properly.

III. NOVEL ZERO-SEQUENCE INJECTION METHODS

Adding high-order harmonics to FFZSI will not affect its power rebalance effort, since these harmonics are expected to generate zero average active power with the fundamental frequency grid currents. In this section, therefore, three new zero-sequence injection methods are described that share the same fundamental frequency component, and only modify the high-order harmonics of the zero-sequence injection.

A. Double 1/6 Third Harmonic Injection (DTHI)

Third harmonic injection is an effective way to improve the dc voltage utilization of the three-phase voltage-source inverter. For symmetrical converter output voltages, a third harmonic injection with an amplitude of 1/6 of the fundamental frequency component achieves the highest ac output voltage without overmodulation [25].

Having noted that FFZSI is also sinusoidal, a straightforward way to find a harmonic injection is to combine the optimal injection of the positive sequence with the optimal one of the zero sequence. The method is hence named as DTHI. The converter output phase voltage of phase a with DTHI can be written as

$$v_a = \underbrace{\sqrt{2}V^+\cos(\omega t+\alpha)}_{\text{Term 1}} - \underbrace{\frac{\sqrt{2}V^+}{6}\cos(3\omega t+3\alpha)}_{\text{Term 2}} + \underbrace{\sqrt{2}V^0\cos(\omega t+\theta)}_{\text{Term 3}} - \underbrace{\frac{\sqrt{2}V^0}{6}\cos(3\omega t+3\theta)}_{\text{Term 4}} \tag{6}$$

where V^+ and V^0 represent the rms value of the positive sequence and zero sequence, respectively. Term 1 in (6) stands for the positive sequence and Term 2 for its 1/6 third harmonic injection, whereas Terms 3 and 4 represent FFZSI and its 1/6 third harmonic injection, respectively.

Implementation of the method is simple, since both the positive sequence and FFZSI are readily available. All that needs to be done is to calculate their 1/6 third harmonic injections. However, one limitation of DTHI is that it is derived based on the assumption that the overall optimal third harmonic injection equals the sum of the optimal injection of its positive sequence and that of its FFZSI. Unfortunately, the superposition principle generally does not apply for this nonlinear situation.

The resultant converter output voltage (phase a) without the third harmonic injection should be the sum of the positive sequence and zero sequence as

$$\begin{aligned} v_a^1 &= \sqrt{2}V_a^1\cos(\omega t+\beta_a) \\ &= \sqrt{2}V^+\cos(\omega t+\alpha)+\sqrt{2}V^0\cos(\omega t+\theta). \end{aligned} \tag{7}$$

However, its optimal third harmonic injection is generally unequal to the sum of the optimal third harmonic injection of its positive sequence and that of its FFZSI

$$-\frac{\sqrt{2}V_a^1}{6}\cos(3\omega t+3\beta_a) \neq -\frac{\sqrt{2}V^+}{6}\cos(3\omega t+3\alpha) - \frac{\sqrt{2}V^0}{6}\cos(3\omega t+3\theta). \tag{8}$$

This demonstrates that, despite its simple implementation and better derivation over FFZSI, DTHI is unable to achieve an optimal implementation and, thus, allows for further improvement.

B. Reduced Third Harmonic Injection (RTHI)

DTHI can be improved by directly deriving the optimal zero-sequence injection of the resultant converter output voltages (sum of the positive sequence and fundamental frequency zero sequence); thus, avoiding separate optimization of third harmonic injections and the superposition.

As we can see from Fig. 5(a), adding the zero sequence v^0 to the symmetrical positive sequence v_a^+, v_b^+, v_c^+ creates a set

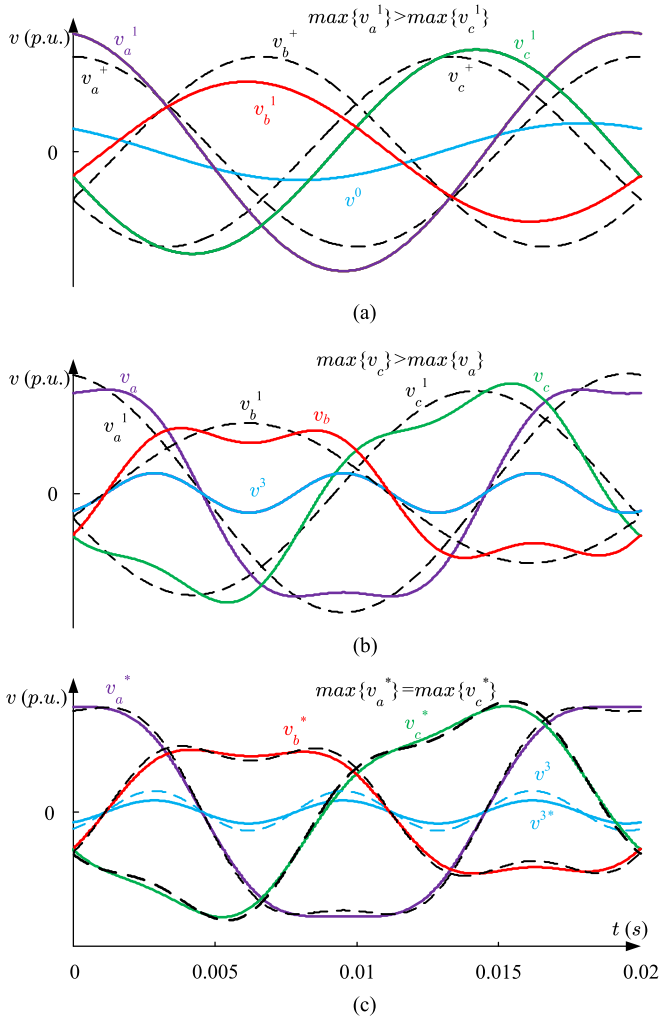

Fig. 5. Problem and solution of RTHI. (a) Positive sequence v_a^+, v_b^+, v_c^+, the zero sequence v_0, and the resultant converter output voltages without third harmonic injection v_a^1, v_b^1, v_c^1. (b) 1/6 third harmonic injection of the phase with largest amplitude v^3 and resultant converter output voltages v_a, v_b, v_c. (c) RTHI v^{3*} and the resultant converter output voltages v_a^*, v_b^*, v_c^*.

of resultant converter output voltages v_a^1, v_b^1, v_c^1, which are still sinusoidal yet asymmetrical as

$$\begin{aligned} v_a^1 &= \sqrt{2}V_a^1\cos(\omega t+\beta_a) \\ &= \sqrt{2}V^+\cos(\omega t+\alpha)+\sqrt{2}V^0\cos(\omega t+\theta) \qquad (9) \\ v_b^1 &= \sqrt{2}V_b^1\cos(\omega t+\beta_b) \\ &= \sqrt{2}V^+\cos(\omega t+\alpha-2\pi/3) \\ &\quad +\sqrt{2}V^0\cos(\omega t+\theta) \qquad (10) \\ v_c^1 &= \sqrt{2}V_c^1\cos(\omega t+\beta_c) \\ &= \sqrt{2}V^+\cos(\omega t+\alpha+2\pi/3) \\ &\quad +\sqrt{2}V^0\cos(\omega t+\theta) \qquad (11) \\ V_a^1 &\neq V_b^1 \neq V_c^1 \qquad (12) \\ \beta_a &\neq \beta_b+2\pi/3 \neq \beta_c-2\pi/3. \qquad (13) \end{aligned}$$

Since the phase with the largest amplitude is most likely to reach the limit set by the dc-side voltages, the third harmonic injection should be calculated based on that phase as

$$v^3 = -\frac{\sqrt{2}V_x^1}{6}\cos(3\omega t+3\beta_x) \qquad (14)$$

where $V_x^1 = \max\{V_a^1, V_b^1, V_c^1\}$. Finally, the converter output voltage of phase a can be written as

$$\begin{aligned} v_a = &\underbrace{\sqrt{2}V^+\cos(\omega t+\alpha)}_{\text{Term 1}} + \underbrace{\sqrt{2}V^0\cos(\omega t+\theta)}_{\text{Term 2}} \\ &\underbrace{-\frac{\sqrt{2}V_x^1}{6}\cos(3\omega t+3\beta_x)}_{\text{Term 3}} \end{aligned} \qquad (15)$$

where Terms 1 and 2 represent the positive sequence and zero sequence, while Term 3 represents the third harmonic injection. With this injection, the most vulnerable phase has been injected with its optimal third harmonics. Fig. 5 illustrates a condition when the method does not work as expected. In the example, phase a has the largest resultant voltage amplitude [see Fig. 5(a)] and, thus, the 1/6 third harmonic of phase a is injected ($V_x^1 = V_a^1$ and $\beta_x = \beta_a$). However, Fig. 5(b) shows that after the injection the largest resultant voltage occurs in phase c, instead of phase a. This is because the three-phase resultant voltages are no longer symmetrical as seen in (11)–(13). The third harmonic injected to reduce the maximum voltage of one phase, in this case, increases the voltage of another phase, contradicting the basic assumption of the method.

Therefore, we have to verify whether the most vulnerable phase remains the same before and after the third harmonic injection. If the phase remains unchanged, the injection given in (14) should be the optimal third harmonic solution. Otherwise, more needs to be done. Reducing the injection level increases the maximum voltage of phase a $v_{a(\max)}$, yet decreases that of phase c $v_{c(\max)}$. Therefore, one way to solve the issue is to reduce the injection level from 1/6 to a proper value, which can be found when the overall maximum voltage $\max\{v_{a(\max)}, v_{c(\max)}\}$ reaches its minimum value, as demonstrated in Fig. 5(c). This is why, this method is called as RTHI. When the aforementioned phenomenon does not happen, the 1/6 third harmonic injection of the phase with the largest amplitude works perfectly. However, when the phenomenon occurs and injection level reduction is necessary, the required computations can make the real-time online calculation challenging.

C. Double Min–Max (DMM)

The min–max sequence is an alternative way to achieve better utilization of the dc voltage, which has equivalent performance to the 1/6 third harmonic injection [25]. By duplicating the idea of DTHI, this section describes the DMM injection, and consists of the min–max sequence of the positive sequence and that of the required fundamental frequency zero sequence (4) as well. The converter output voltage of phase a with DMM can be

expressed as

$$v_a = \underbrace{\sqrt{2}V^+\cos(\omega t+\alpha)}_{\text{Term 1}} + \underbrace{\min\max\left\{v_a^+, v_b^+, v_c^+\right\}}_{\text{Term 2}} + \underbrace{\sqrt{2}V^0\cos(\omega t+\theta)}_{\text{Term 3}} + \underbrace{\min\max\left\{v^0, v^{0*}, v^{0**}\right\}}_{\text{Term 4}} \quad (16)$$

where

$$\min\max\left\{v_a^+, v_b^+, v_c^+\right\} = -\frac{\min\left\{v_a^+, v_b^+, v_c^+\right\} + \max\left\{v_a^+, v_b^+, v_c^+\right\}}{2} \quad (17)$$

$$\min\max\left\{v^0, v^{0*}, v^{0**}\right\} = -\frac{\min\left\{v^0, v^{0*}, v^{0**}\right\} + \max\left\{v^0, v^{0*}, v^{0**}\right\}}{2} \quad (18)$$

$$v_a^+ = \sqrt{2}V^+\cos(\omega t+\alpha) \quad (19a)$$

$$v_b^+ = \sqrt{2}V^+\cos(\omega t+\alpha-2\pi/3) \quad (19b)$$

$$v_c^+ = \sqrt{2}V^+\cos(\omega t+\alpha+2\pi/3) \quad (19c)$$

$$v^0 = \sqrt{2}V^0\cos(\omega t+\theta) \quad (20a)$$

$$v^{0*} = \sqrt{2}V^0\cos(\omega t+\theta-2\pi/3) \quad (20b)$$

$$v^{0**} = \sqrt{2}V^0\cos(\omega t+\theta+2\pi/3). \quad (20c)$$

Terms 1 and 3 represent the positive sequence and the fundamental frequency zero sequence, respectively, while Terms 2 and 4 represent the min–max sequence of the positive sequence and zero sequence, respectively. v^{0*} and v^{0**} are fictitious voltages created by displacing v^0 by 120° and 240°, respectively, because the min–max sequence can only be calculated with a set of three-phase voltages.

DMM separately derives the min–max sequence injections of the positive sequence and the fundamental frequency zero sequence and then superposes, just as in DTHI. However, unlike DTHI, the superposition principle works well for DMM. The min–max sequence is calculated based on the instantaneous values of a set of three-phase voltages, and separate derivation of the min–max sequence of the positive sequence and the fundamental frequency zero-sequence component is allowed.

IV. Simulation Verification

A 10-MW three-phase seven-level CHB converter was simulated using MATLAB/PLECS to verify the effectiveness of the proposed methods. The parameters of the converter are listed in Table II. The converter enables a direct connection to the 6.6-kV distribution network without a line frequency power transformer. The capacitor voltage of each H-bridge is regulated to be constant at 2200 V. In real applications, the voltage could be lower if more H-bridges were cascaded. The multilevel waveform synthesis allows the switching frequency to be as low as 600 Hz, greatly reducing switching losses. The selected PV module (BP365) reaches a maximum power output of 65 W under an irradiance of 1000 W/m^2. Each H-bridge is fed by a 1.11-MW PV block, which is formed by the series and parallel connection of modules in the way listed in Table III.

TABLE II
Simulation Parameters of the Three-phase Seven-Level CHB Converter

Parameters	Values
Three-phase Nominal Power $P_{\rm nom}$	10 MW
Grid Voltage V_g	6600 V
Capacitor Voltage $v_{\rm dc}$	2200 V
IGBT Voltage Rating	3300 V
IGBT Current Rating	1500 A
Filtering Inductor L_f	5 mH
Phase Shift PWM Carrier Frequency f_s	600 Hz

TABLE III
PV Parameters

Parameters	Values
PV Module Type	BP 365
Output Voltage at Maximum Power Point	17.65 V
Output Current at Maximum Power Point	3.68 A
Maximum Power	65 W
Series PV Modules per String	55
Paralleled Strings per H-Bridge	311

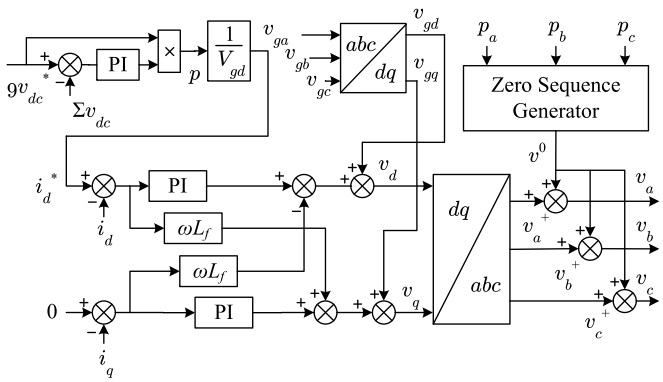

Fig. 6. Control implementation.

A conventional decoupled control based on the *dq* rotational frame (see Fig. 6) is implemented. The sum of capacitor voltages is regulated toward the reference by amplifying the error signal and setting it as the direct axis current reference. The zero sequence v^0, which is the focus of this paper, is generated based on three-phase power generation p_a, p_b, p_c with the methods described above, and added to the converter output voltages.

A. Case I ($\lambda_a = 1, \lambda_b = 0.7929, \lambda_c = 1$)

It is assumed that the irradiance on the PV modules of phase b falls from 1000 to 800 W/m^2, corresponding to 79.29% of its peak power, whereas the other two phases are subject to uniform irradiance of 1000 W/m^2. If unregulated, the grid current

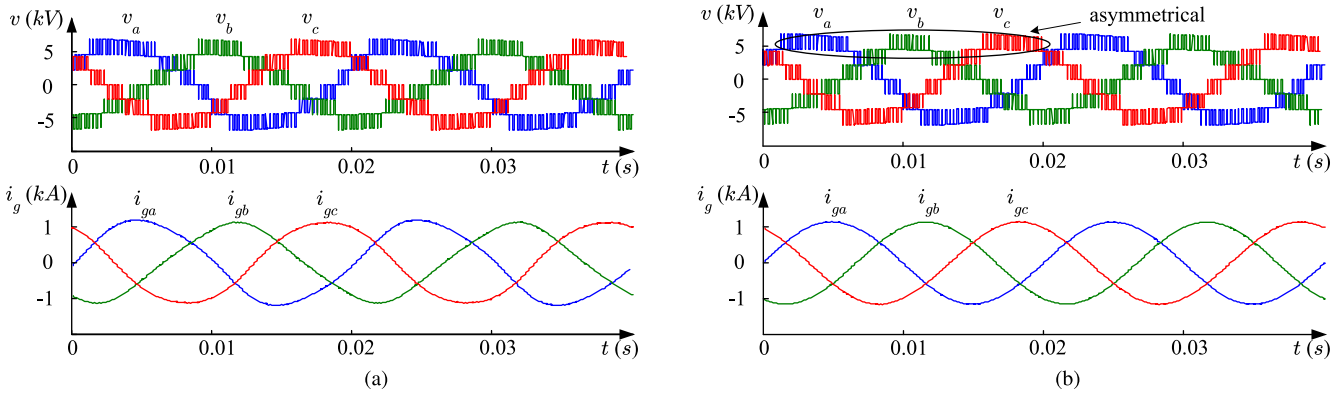

Fig. 7. Simulation results of converter output voltages v_a, v_b, v_c and grid currents i_{ga}, i_{gb}, i_{gc} of unbalanced operation Case I with: (a) unregulated and (b) FFZSI.

TABLE IV
CURRENT IMBALANCE AND DISTORTION (CASE I) (SIMULATION)

Methods	Imbalance	Distortion		
	±	THD (i_{ga})	THD (i_{gb})	THD (i_{gc})
Unregulated	5.61%	5.05%	5.19%	4.35%
FFZSI	0.15%	0.74%	0.73%	0.80%

imbalance and harmonic distortion will be unacceptable [see Fig. 7(a)]. Results with FFZSI under the same power imbalance are shown in Fig. 7(b). The converter output voltages become asymmetrical to maintain three-phase balanced grid currents. The current imbalance, which is indicated by comparing the amplitude of the negative sequence to that of the positive sequence [26] and total harmonic distortion (THD) are listed in Table IV.

B. *Case II* ($\lambda_a = 0.3813, \lambda_b = 0.4834, \lambda_c = 0.6894$)

In the second case, the irradiance on the PV modules of phase a, phase b, and phase c drops to 400, 500, and 700 W/m^2, corresponding to 38.13%, 48.34%, 68.94% of its peak power, respectively. It is shown in Fig. 8(a) that the FFZSI results in considerable harmonic distortion with the grid currents due to converter saturation. The imbalance also increases as power redistribution cannot be implemented satisfactorily in the overmodulation region. The current imbalance and distortion for Case II are demonstrated in Table V. The three presented methods (DTHI, RTHI, and DMM), on the other hand, are still able to generate balanced grid currents with acceptable level of harmonic distortion, despite the deteriorated power imbalance [see Fig. 8(b)–(d)]. Their superior performance in achieving three-phase balanced grid currents is hence confirmed.

V. EXPERIMENTAL RESULTS

Fig. 9 shows the schematic diagram and hardware image of the 8-kW three-phase seven-level CHB converter designed, constructed and tested in the laboratory to verify the feasibility of proposed methods (Case I) and their superiority compared to the conventional solution (Case II).

The prototype is fed by nine isolated Elgar TerraSAS PV simulators from Ametek, each of which is rated at 600 V and 8 A. The profile of the Sunpower 230 (72 cells) PV module is used in the PV simulators. In this experiment, each simulator is programmed to simulate the electrical behavior of a string consisting of four PV modules in series. The maximum power output of 920 W (164 V and 5.61 A) is expected for each bridge under 1000 W/m^2 and 25 °C. With a total of nine bridges, the converter thus delivers the peak power of 8 kW into the grid. Nine Powerex H-bridge modules (PP75B060) rated at 600 V 75 A are used to construct the three-phase seven-level converter. In this experiment, the capacitor voltage is designed to be fixed at 164 V, which tracks the maximum power point under 1000 W/m^2 and 25 °C. Each module comes with electrolytic capacitors with a capacitance value of 18 mF, which corresponds to a unit capacitance constant H of 270 ms at 164 V [27].

The control strategy is implemented in a dSPACE DS1006 platform with onboard Xilinx FPGA modules operating at 100 MHz to ensure a real-time PWM generation. The carrier frequency of the phase-shifted PWM is chosen to be 600 Hz, representing a switching frequency practical for real applications. Since three H-bridges are cascaded in one phase leg, the converter output phase voltages feature seven-level waveforms with an equivalent switching frequency of 3.6 kHz. Finally, the prototype is connected to the 430-V three-phase utility grid via an isolation transformer.

The dc–dc conversion, which should be included in real applications, is omitted in the setup, since the focus of the paper lies in the interphase power balance, and galvanic isolation has already been implemented internally in the PV simulators. The only problem that may arise without those dc–dc converters is the inability to accurately track the maximum power point, when it moves as a result of changes in irradiance or temperature, but it does not affect the purpose of this paper to demonstrate zero-sequence injection methods.

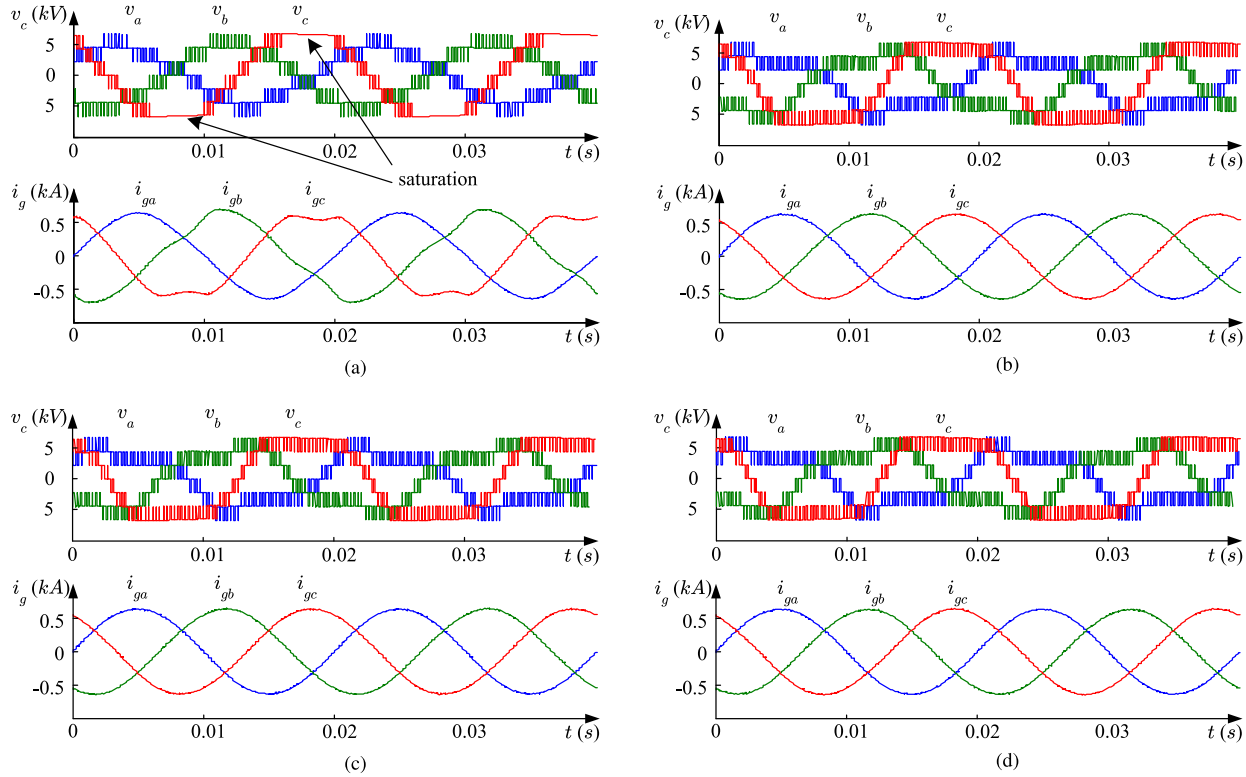

Fig. 8. Simulation results of converter output voltages v_a, v_b, v_c and grid currents i_{ga}, i_{gb}, i_{gc} of unbalanced operation Case II with: (a) FFZSI, (b) DTHI, (c) RTHI, and (d) DMM.

TABLE V
CURRENT IMBALANCE AND DISTORTION (CASE II) (SIMULATION)

Methods	Imbalance ±	Distortion THD (i_{ga})	THD (i_{gb})	THD (i_{gc})
FFZSI	2.15%	3.33%	9.40%	11.95%
DTHI	0.31%	1.40%	1.66%	1.32%
RTHI	0.30%	1.41%	1.66%	1.33%
DMM	0.59%	1.25%	1.46%	1.42%

Fig. 10(a) shows the experimental results when all PV strings are subject to 1000 W/m^2 and 25 °C to demonstrate the balanced operation of the CHB converter prototype. The converter output voltages feature seven-level synthesized waveforms, as expected, and grid currents are symmetrical with limited harmonics. The dc-side voltages and currents of three bridges ($a1$, $b1$, $c1$) are shown in Fig. 11(a) to confirm the balanced power generation among all phases. The voltages and currents of the other six bridges are not included here, as no interbridge power imbalance is introduced.

A. *Case I* ($\lambda_a \approx 0.8$, $\lambda_b = 1$, $\lambda_c = 1$)

The solar irradiance level was decreased from 1000 to 800 W/m^2 in phase a, corresponding to approximately 80% of its peak power. The irradiance levels in the simulators of phases b and c remained at 1000 W/m^2.

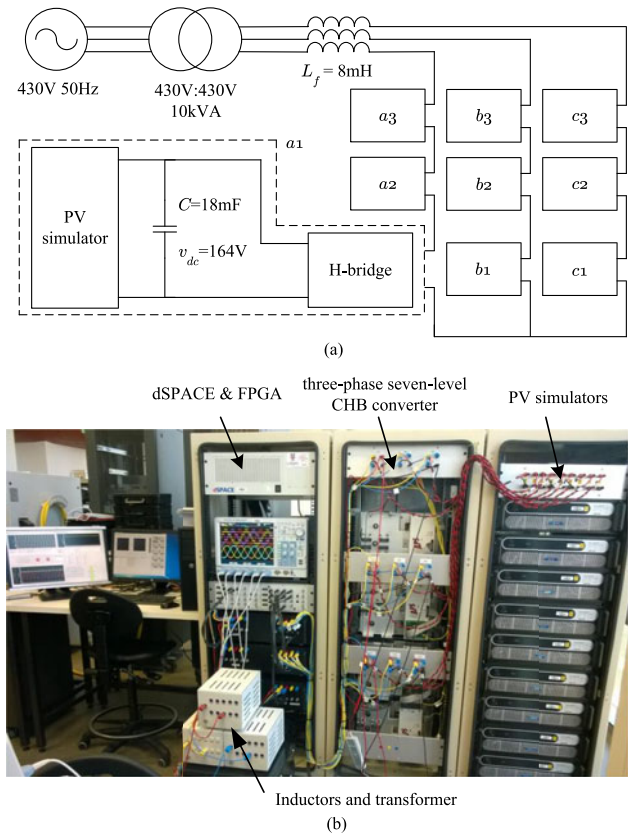

Fig. 9. Experimental setup: (a) schematic diagram, and (b) hardware image.

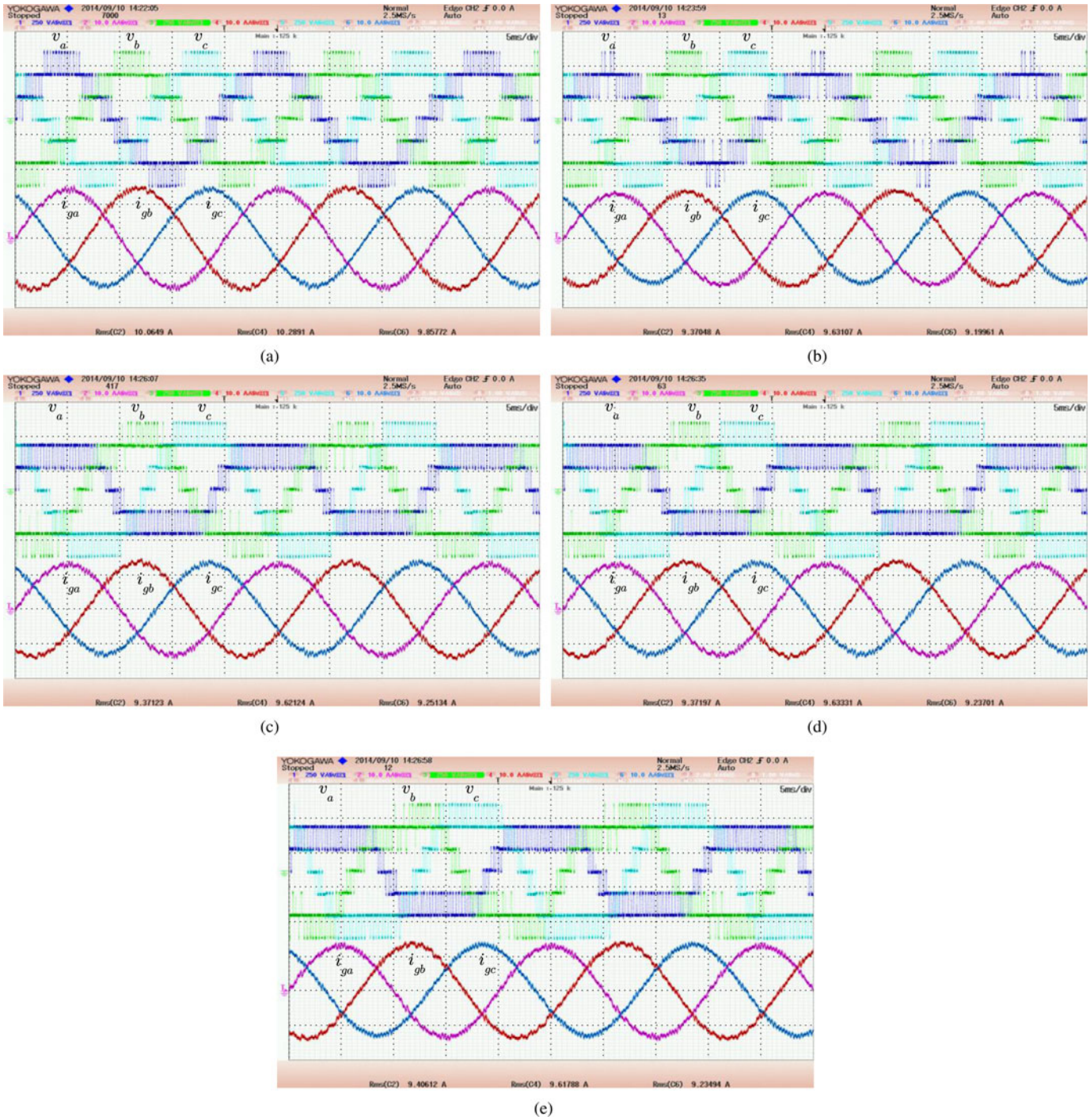

Fig. 10. Experimental results of converter output voltages and grid currents of: (a) balanced operation, (b) unbalanced operation Case I with FFZSI, (c) unbalanced operation Case I with DTHI, (d) unbalanced operation Case I with RTHI, (e) unbalanced operation Case I with DMM. CH1: converter output voltage of phase a v_a; CH2: grid current of phase a i_{ga}; CH3: converter output voltage of phase b v_b; CH4: grid current of phase b i_{gb}; CH5: converter output voltage of phase c v_c; CH6: grid current of phase c i_{gc}. CH1, CH3, CH5: 250 V/div; CH2, CH4, CH6: 10 A/div.

Fig. 10(b) shows the results with FFZSI. The three-phase converter output voltages v_a, v_b, v_c are no longer symmetrical, owing to the injection of the zero sequence and the shift of the neutral point. However, only this way can the converter deliver three-phase balanced currents into the grid. The experimental waveforms with DTHI, RTHI, and DMM under the same power imbalance are demonstrated in Fig. 10(c)–(e), respectively, to verify the feasibility of these methods. The

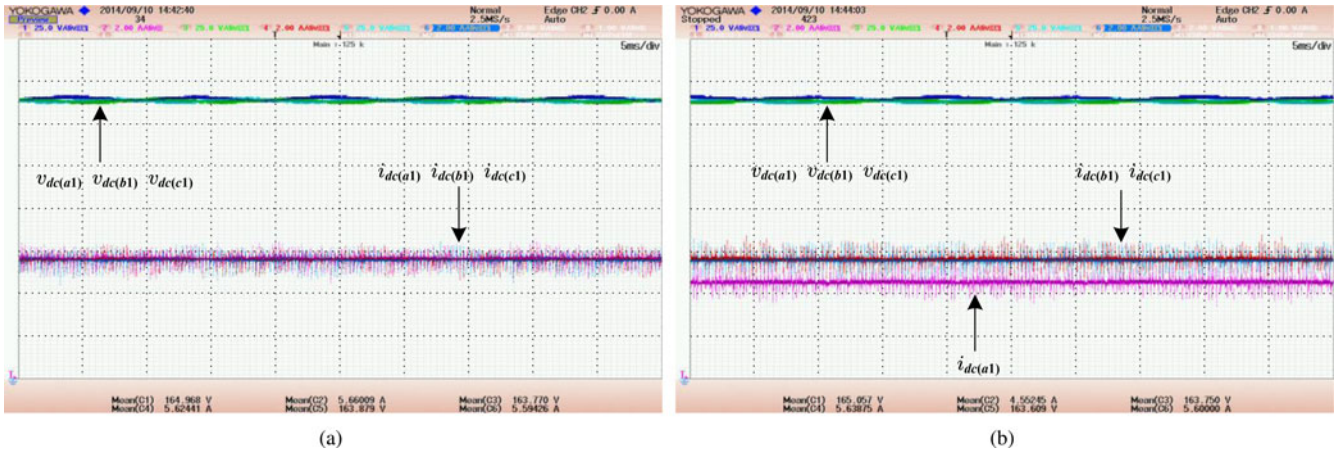

Fig. 11. Experimental results of selected dc-side voltages and currents with: (a) balanced operation, (b) unbalanced operation Case I with FFZSI. CH1: capacitor voltage of Bridge A1 $v_{\mathrm{dc}(a1)}$; CH2: dc current of Bridge A1 $i_{\mathrm{dc}(a1)}$; CH3: capacitor voltage of Bridge B1 $v_{\mathrm{dc}(b1)}$; CH4: dc current of Bridge B1 $i_{\mathrm{dc}(b1)}$; CH5: capacitor voltage of Bridge C1 $v_{\mathrm{dc}(c1)}$; CH6: dc current of Bridge C1 $i_{\mathrm{dc}(c1)}$. CH1, CH3, CH5: 25 V/div; CH2, CH4, CH6: 2 A/div.

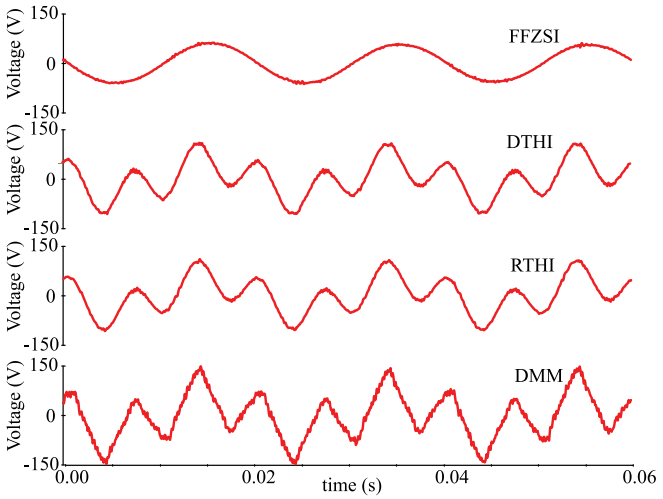

Fig. 12. Experimentally measured injections of FFZSI, DTHI, RTHI, and DMM.

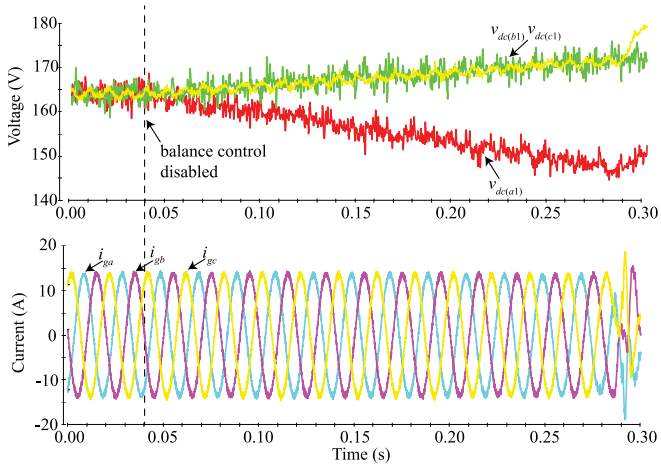

Fig. 13. Experimental results of capacitor voltages and grid currents after disabling FFZSI.

converter output voltages feature different waveforms owing to the injection of different zero sequences, and the grid currents are balanced as expected.

The unique characteristics of each zero-sequence injection are further illustrated Fig. 12. Although the waveforms differ in shape, all zero-sequence injections share the same fundamental frequency component, which is uniquely defined by the power imbalance in (5).

The dc-side voltages and currents of bridges $a1, b1, c1$ under these irradiance levels are shown in Fig. 11(b) to confirm the unbalanced operation. Although bridge $a1$ generates 20% less power than bridges $b1$ and $c1$, all capacitor voltages can still be regulated around the reference value. If the balance algorithm (FFZSI) is disabled, the capacitor voltages will diverge from the reference, as demonstrated in Fig. 13. This is because, without power balancing control, the converter collects equal amounts of power from the H-bridges, whereas the power generated by the respective PV simulators connected to those H-bridges may not be equal. When the capacitor voltages (in this case $v_{\mathrm{dc}(a1)}$, $v_{\mathrm{dc}(a2)}$, $v_{\mathrm{dc}(a3)}$) decrease to the level lower than the peak value of the converter output voltages, the converter loses the ability to regulate the grid currents.

B. Case II ($\lambda_a \approx 0.45$, $\lambda_b = 1$, $\lambda_c = 1$)

The irradiance level of the PV simulators connected to phase a was further decreased to 450 W/m^2, while the other two phases were left unaltered at 1000 W/m^2. The grid current waveforms with FFZSI, DTHI, RTHI, and DMM are depicted in Fig. 14. These results demonstrate that, under this power imbalance,

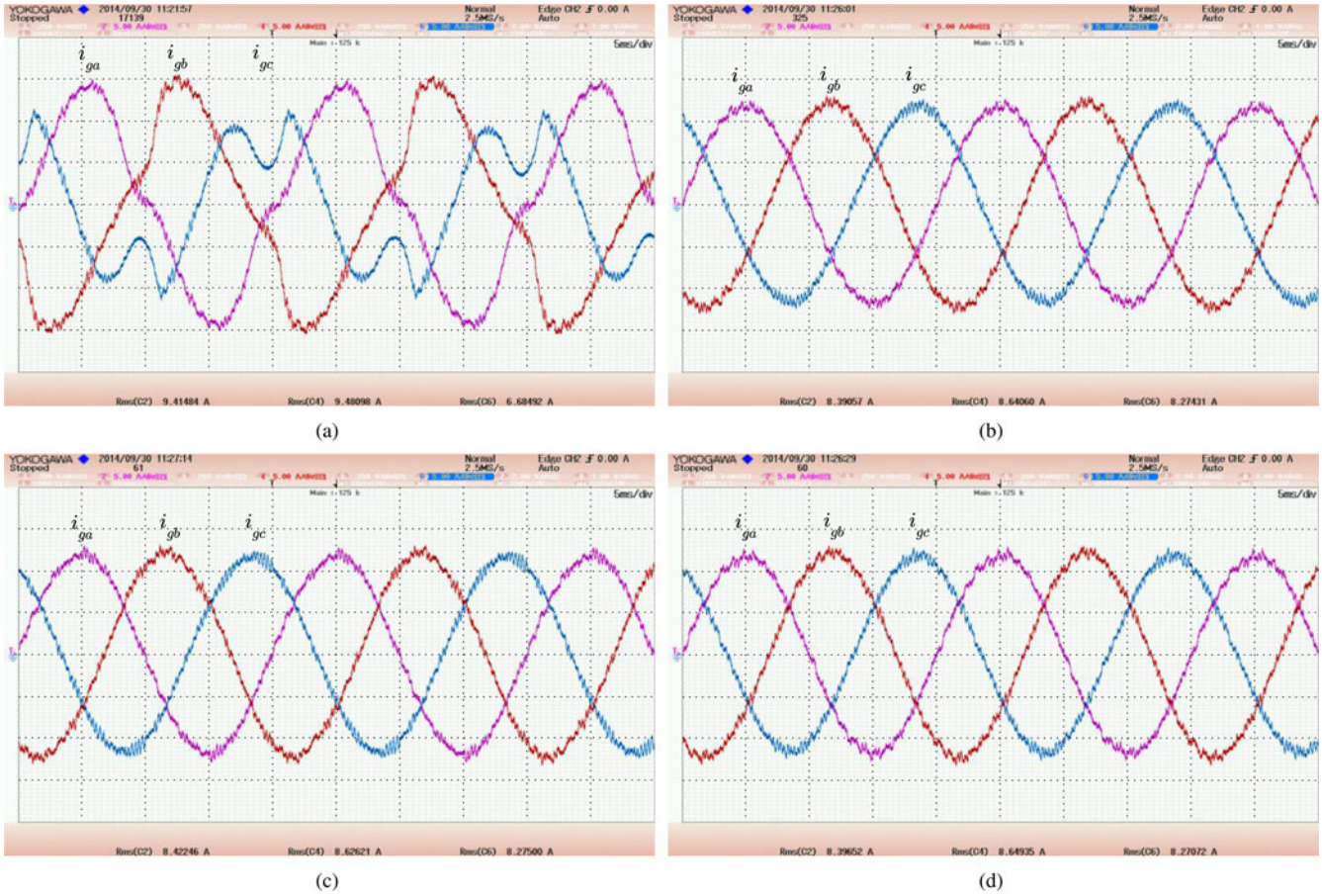

Fig. 14. Experimental results of grid currents of unbalanced operation Case II with: (a) FFZSI, (b) DTHI, (c) RTHI, (d) DMM. CH2: grid current of phase a i_{ga}; CH4: grid current of phase b i_{gb}; CH6: grid current of phase c i_{gc}. CH2, CH4, CH6: 5 A/div.

FFZSI fails to provide three-phase balanced grid currents due to converter saturation, while DTHI, RTHI, and DMM all exhibit a satisfactory performance. The results confirm the superiority of the proposed methods over FFZSI for severe power imbalance conditions.

VI. Conclusion

Injection of a zero sequence is necessary in order to deal with interphase power imbalance in a CHB converter. In addition to the existing FFZSI method, three novel methods have been proposed in this paper, i.e., DTHI, RTHI, and DMM zero-sequence injection. They share the same fundamental frequency component with FFZSI, although their high-order harmonic components are different. The proposed methods are able to rebalance the grid currents under severe interphase power imbalance conditions, where conventional FFZSI fails; thus, effectively extending the power balance limit of a CHB converter. DTHI and DMM also feature simple implementation. Both simulation and experimental results have been provided to validate the feasibility and superiority of the proposed methods.

References

[1] Z. Moradi-Shahrbabak, A. Tabesh, and G. R. Yousefi, "Economical design of utility-scale photovoltaic power plants with optimum availability," *IEEE Trans. Ind. Electron.*, vol. 61, no. 7, pp. 3399–3406, Jul. 2014.

[2] M. Morjaria, D. Anichkov, V. Chadliev, and S. Soni, "A grid-friendly plant: The role of utility-scale photovoltaic plants in grid stability and reliability," *IEEE Power Energy Mag.*, vol. 12, no. 3, pp. 87–95, May/Jun. 2014.

[3] P. Denholm, R. Margolis, T. Mai, G. Brinkman, E. Drury, M. Hand, and M. Mowers, "Bright future: Solar power as a major contributor to the U.S. grid," *IEEE Power Energy Mag.*, vol. 11, no. 2, pp. 22–32, Mar./Apr. 2013.

[4] T. Kerekes, E. Koutroulis, D. Séra, D. R. Teodorescu, and M. Katsanevakis, "An optimization method for designing large PV plants," *IEEE J. Photovoltaics*, vol. 3, no. 2, pp. 814–822, Apr. 2013.

[5] J. Carrasco, L. Franquelo, J. Bialasiewicz, E. Galvan, R. Guisado, M. Prats, J. Leon, and N. Alfonso, "Power-electronic systems for the grid integration of renewable energy sources: A survey," *IEEE Trans. Ind. Electron.*, vol. 53, no. 4, pp. 1002–1016, Jun. 2006.

[6] SMA Sunny Central 800CPXT/850CPXT/900CPXT. (2013). [Online]. Available: http://files.sma.de/dl /18859/SC800CP-900CPDEN131915 W.pdf

[7] ABB central inverters PVS800 100 to 1000 kW. (2013). [Online]. Available: http://www05.abb.com /global/scot/scot232.nsf/veritydisplay/ 2d8c5c00c2efeee4c1257ceb002b428 9$file/17135_PVS800_central_inverters_flyer_EN_3AUA0000057380 _RevK_lowres.pdf

[8] S. Kouro, M. Malinowski, K. Gopakumar, J. Pou, L. Franquelo, B. Wu, J. Rodriguez, M. Perez, and J. Leon, "Recent advances and industrial

applications of multilevel converters," *IEEE Trans. Ind. Electron.*, vol. 57, no. 8, pp. 2553–2580, Aug. 2010.

[9] M. Cavalcanti, A. Farias, K. Oliveira, and J. Afonso, "Eliminating leakage currents in neutral point clamped converters for photovoltaic systems," *IEEE Trans. Ind. Electron.*, vol. 59, no. 1, pp. 435–443, Jan. 2012.

[10] S. Monge, J. Rocabert, P. Rodriguez, S. Alepuz, and J. Bordonau, "Multilevel diode-clamped converter for photovoltaic generators with independent voltage control of each solar array," *IEEE Trans. Ind. Electron.*, vol. 55, no. 7, pp. 2713–2723, Jul. 2008.

[11] M. R. Islam, Y. Guo, and J. Zhu, "A high-frequency link multilevel cascaded medium-voltage converter for direct grid integration of renewable energy systems," *IEEE Trans. Power Electron.*, vol. 29, no. 8, pp. 4167–4182, Aug. 2014.

[12] J. Sastry, P. Bakas, H. Kim, L. Wang, and A. Marinopoulos, "Evaluation of cascaded H-bridge inverter for utility-scale photovoltaic systems," *Renew. Energy*, vol. 69, pp. 208–218, Sep. 2014.

[13] D. Sun, B. Ge, X. Yan, D. Bi, H. Zhang, Y. Liu, H. Abu-Rub, L. Ben-Brahim, and F. Z. Peng, "Modeling, impedance design, and efficiency analysis of quasi-Z Source module in cascaded multilevel photovoltaic power system," *IEEE Trans. Ind. Electron.*, vol. 61, no. 11, pp. 6108–6117, Nov. 2014.

[14] W. Zhao, H. Choi, G. Konstantinou, M. Ciobotaru, and V. Agelidis, "Cascaded H-bridge multilevel converter for large-scale PV grid-integration with isolated DC-DC stage," in *Proc. IEEE Power Electron. Distrib. Gener. Syst. Conf.*, 2012, pp. 849–856.

[15] E. Villanueva, P. Correa, J. Rodriguez, and M. Pacas, "Control of a single-phase cascaded H-bridge multilevel converter for grid-connected photovoltaic systems," *IEEE Trans. Ind. Electron.*, vol. 56, no. 11, pp. 4399–4406, Nov. 2009.

[16] J. Chavarria, D. Biel, F. Guinjoan, C. Meza, and J. Negroni, "Energy-balance control of PV cascaded multilevel grid-connected converters under level-shifted and phase-shifted PWMs," *IEEE Trans. Ind. Electron.*, vol. 60, no. 1, pp. 98–111, Jan. 2013.

[17] C. Townsend, T. Summers, and R. Betz, "Control and modulation scheme for a cascaded H-bridge multi-level converter in large scale photovoltaic systems," in *Proc. IEEE Energy Convers. Congr. Expo.*, 2012, pp. 3707–3714.

[18] Y. Yu, G. Konstantinou, B. Hredzak, and V. Agelidis, "On extending the energy balancing limit of multilevel cascaded H-bridge converters for large-scale photovoltaic farms," in *Proc. Australas. Univ. Power Eng. Conf.*, 2013, pp. 1–6.

[19] S. Rivera, B. Wu, S. Kouro, and D. Zhang, "Cascaded H-bridge multilevel converter topology and three-phase balance control for large scale photovoltaic systems," in *Proc. IEEE Power Electron. Distrib. Gener. Syst. Conf.*, 2012, pp. 690–697.

[20] B. Xiao, L. Hang, J. Mei, C. Riley, L. Tolbert, and B. Ozpineci, "Modular cascaded H-bridge multilevel PV inverter with distributed MPPT for grid-connected applications," *IEEE Trans. Ind. Appl.*, to be published.

[21] L. Liu, H. Li, Y. Xue, and W. Liu, "Reactive power compensation and optimization strategy for grid-interactive cascaded photovoltaic systems," *IEEE Trans. Power Electron.*, vol. 30, no. 1, pp. 188–202, Jan. 2015.

[22] J. Mei, B. Xiao, K. Shen, L. M. Tolbert, and J. Y. Zheng, "Modular multilevel inverter with new modulation method and its application to photovoltaic grid-connected generator," *IEEE Trans. Power Electron.*, vol. 28, no. 11, pp. 5063–5073, Nov. 2013.

[23] S. Essakiappan, H. S. Krishnamoorthy, P. Enjeti, R. S. Balog, and S. Ahmed, "Multilevel medium frequency link inverter for utility scale photovoltaic integration," *IEEE Trans. Power Electron.*, vol. 30, no. 7, pp. 3674–3684, Jul. 2015.

[24] *IEEE Standard for Interconnecting Distributed Resources With Electric Power Systems*, IEEE Standard 1547, 2003.

[25] D. Holmes and T. A. Lipo, *Pulse Width Modulation for Power Converters: Principles and Practice*, 3rd ed. New York, NY, USA: Wiley, 2003, pp. 226–230, 270–272.

[26] IEEE *Recommended Practice for Monitoring Electric Power Quality*, IEEE Standard 1159-2009, 2009.

[27] H. Akagi, S. Inoue, and T. Yoshii, "Control and performance of a transformerless cascade PWM STATCOM with star configuration," *IEEE Trans. Ind. Appl.*, vol. 43, no. 4, pp. 1041–1049, Jul./Aug. 2007.

Yifan Yu (S'13) received the B.Eng. and M.Eng. degrees in electrical engineering from the Harbin Institute of Technology, Harbin, China, in 2010 and 2012, respectively. He is currently working toward the Ph.D. degree at the University of New South Wales, Sydney, N.S.W., Australia.

His research interests include multilevel converters, Z-Source inverters, photovoltaic grid connection, and other aspects of power electronic technology for renewable energy sources.

Georgios Konstantinou (S'08–M'13) received the B.Eng. degree in electrical and computer engineering from the Aristotle University of Thessaloniki, Thessaloniki, Greece, in 2007, and the Ph.D. degree in electrical engineering from the University of New South Wales (UNSW), Sydney, N.S.W., Australia, in 2012.

He is currently a Senior Research Associate with the Australian Energy Research Institute and the School of Electrical Engineering and Telecommunications, UNSW. He is an Associate Editor of the *IET Power Electronics*. His research interests include hybrid and modular multilevel converters, pulse width modulation, and selective harmonic elimination techniques for power electronics.

Branislav Hredzak (M'98–SM'13) received the B.Sc./M.Sc. degree from the Technical University of Kosice, Kosice, Slovakia, in 1993, and the Ph.D. degree from the Napier University of Edinburgh, Edinburgh, U.K., in 1997, all in electrical engineering.

He was as a Lecturer and a Senior Researcher in Singapore from 1997 to 2007. He is currently a Senior Lecturer at the School of Electrical Engineering and Telecommunications, University of New South Wales, Sydney, N.S.W., Australia. His current research interests include hybrid storage technologies and advanced control systems for power electronics and storage systems.

Vassilios G. Agelidis (S'89–M'91–SM'00) was born in Serres, Greece. He received the B.Eng. degree in electrical engineering from the Democritus University of Thrace, Thrace, Greece, in 1988, the M.S. degree in applied science from Concordia University, Montreal, QC, Canada, in 1992, and the Ph.D. degree in electrical engineering from Curtin University, Perth, W.A., Australia, in 1997.

He was with Curtin University from 1993 to 1999; with the University of Glasgow, Glasgow, U.K., from 2000 to 2004; with Murdoch University, Perth, from 2005 to 2006; and the University of Sydney, Sydney, N.S.W., Australia, from 2007 to 2010. He is currently the Director of the Australian Energy Research Institute, School of Electrical Engineering and Telecommunications, University of New South Wales, Sydney.

Prof. Agelidis received the Advanced Research Fellowship from the U.K. Engineering and Physical Sciences Research Council in 2004. He was the Vice-President for Operations with the IEEE Power Electronics Society from 2006 to 2007. He was an AdCom Member of the IEEE PELS from 2007 to 2009 and the Technical Chair of the 39th IEEE Power Electronics Specialists Conference in 2008 held in Rhodes, Greece.